Angewandte
Eine Zeitschrift der Gesellschaft Deutscher Chemiker
Chemie

Supporting Information

GM_1 Ganglioside Inhibits β-Amyloid Oligomerization Induced by Sphingomyelin

Mariana Amaro, Radek Šachl, Gokcan Aydogan, Ilya I. Mikhalyov, Robert Vácha, and Martin Hof**

anie_201603178_sm_miscellaneous_information.pdf

SUPPLEMENTARY INFORMATION

Table of contents

Experimental Methods

$A\beta_{40}$ peptides preparation: $A\beta_{40}$ peptides tagged with HiLyteFluor488 (g-Aβ) or HiLyteFluor647 (r-Aβ) were purchased from AnaSpec (Fremont, CA, USA) and hexafluoroisopropanol (HFIP) was purchased from Sigma-Aldrich (St. Louis, MO, USA). To prepare monomeric peptide solutions, the Aβ powder was dissolved in pure HFIP to a concentration of 10^{-4}M and sonicated for at least 10 minutes. The solution was then divided into nanomol aliquots and stored in Eppendorf LoBind microcentrifuge tubes. The alcohol was allowed to evaporate under a Nitrogen flow and the resulting peptide films were dried under vacuum for thorough HFIP removal. The aliquots were then stored at -20ºC. To prepare an Aβ solution an aliquot was taken and allowed to stabilize thermally at room temperature prior to opening. The peptide film was then directly re-suspended in glucose buffer (~ 80 mM glucose, 10 mM HEPES and 10 mM NaCl, pH 7.2, osmolarity: 103 $mOsm.kg^{-1}$). Each Aβ solution was prepared directly before measurements. The final concentration of Aβ in all samples was 12 nM.

Giant Unilamellar Vesicle preparation: 1,2-dioleoyl-*sn*-glycero-3-phosphocholine (DOPC), 1-palmitoyl-2-oleoyl-*sn*-glycero-3-phosphocholine (POPC), 1-oleoyl-2-stearoyl-*sn*-glycero-3-phosphocholine (OSPC), 1,2-distearoyl-*sn*-glycero-3-phosphocholine (DSPC), GM_1 Ganglioside (Ovine brain sodium salt), cholesterol (Chol), N-stearoyl-D-erythro-sphingosylphosphorylcholine (Sph) and 1,2-dipalmitoyl-*sn*-glycero-3-phosphoethanolamine-N-(cap biotinyl) (biotinyl Cap PE) were purchased from Avanti Polar Lipids (Alabaster, AL, U.S.A.) and used without further purification. DiIC18(5)-DS (DiD) was purchased from Invitrogen (Carlsbad, CA, USA). Streptavidin and biotin labeled bovine serum albumin (biotin-BSA), were purchased from Sigma (St. Louis, MO, USA). Synthesis of FL-BODIPY-GM_1 (g-GM_1) and of 564/570-bodipy-GM_1 (r-GM_1) is described elsewhere [1]. GUVs were prepared by the electroformation method [2] using titanium chambers. Compositions of GUVs in total mol % for samples containing GM_1 are detailed in **Suplementary Note 4 (Tables S23, S24 and S25)**. Lipid mixtures of 100 nmol in 100 μL of chloroform were made from stock solutions in chloroform. For FCS experiments the probe-to-lipid ratio was approximately 1:100000. For FRET experiments the donor(acceptor)-to-lipid ratio for the g-GM_1/DiD pair was 1:1000 (1:200) and for the g-GM_1/r-GM_1 pair it was 1:200 for both donor and acceptor. All lipid mixtures contained 2nmol of biotinyl Cap PE for immobilization of GUVs (at max 2 mol % of total lipid composition). The lipid solution was spread onto two hollowed titanium plates, which were placed on a heating plate at approximately 47°C to facilitate solvent evaporation. The plates were then put in vacuum for at least 1 h to promote evaporation of remaining traces of solvent. The lipid-coated plates were assembled using one layer of parafilm for insulation and the chamber was filled with 1 ml preheated sucrose solution (100 mM sucrose, and osmolarity of 103 $mOsm.kg^{-1}$). The assembled plates were placed on a heating plate at approximately 47°C and an alternating electrical field of 10 Hz was applied. During the first 45 min the voltage was increased step-wise from 0.150 V to 1.1 V (peak-to-peak voltage) and then kept at 1.1 V for 2.5 h. Finally, the current was set to 4 Hz and 1.3 V for 30 min in order to detach the formed liposomes.

Sample preparation: 20 μL of the GUVs suspension were placed on a microscopy chamber, coated with BSA-biotin/streptavidin for immobilization of the GUVs, containing glucose buffer. The solutions of monomeric Aβ peptides were added to the chambers to a final concentration of 12nM. Aβ peptide to total lipid in chamber ratio was estimated to be 1:4000 (0.02 mol %) at maximum. The samples were allowed to incubate for 10 min before the first measurements. Experiments were performed at 26ºC.

Analytical ultracentrifugation: Sedimentation velocity experiments were performed using a ProteomeLab XL I Beckman Coulter analytical ultracentrifuge equipped with an AN50Ti rotor. Samples of g-Aβ were prepared in glucose buffer as described above. Buffer density, viscosity and partial specific volume of analyzed peptide were estimated using the program SEDNTERP 1.09 (www.jphilo.mailway.com/download.htm). Data analysis was performed with the SEDFIT package [3]. Experiments were conducted at loading concentrations of 1.5, 3.0 and 4.3 μM, at 20°C, with rotor speeds of 48,000 rpm. Scans were recorded at 649 nm in 1 min intervals with 30 μm spatial resolution. Sedimentation velocity data were analyzed using a sedimentation coefficient distribution model c(s). Peaks were integrated to determine the weight-averaged sedimentation coefficients s_w.

FLIM-FRET, Z-scan FCS and FCCS: measurements were performed on a home-built confocal microscope consisting of an inverted confocal microscope body IX71 (Olympus, Hamburg, Germany). Pulsed diode lasers (LDH-P-C-470, 470 nm, and LDH-D-C-635, 635 nm; PicoQuant, Berlin, Germany) were used at 10 MHz repetition rate each and pulsed alternatively. Laser light was coupled to a polarization maintaining single mode optical fiber and re-collimated at the output with an air space objective (UPLSAPO 4X). The light was up-reflected with a 470/635 dichroic mirror onto a water immersion objective (UPLSAPO 60x, Olympus). The fluorescence signal was split between two single photon avalanche diodes using 515/50 and 697/58 band pass filters (Chroma Rockingham, VT) for the green and red channels, respectively.

2-colour FCS: laser intensity at the back aperture of the objective was approximately 10 μW for each laser. Measurements were performed on the top of selected GUVs. For z-scans, the membrane was first placed on the waist of the focus of the laser and then moved 1.4 μm above it. A sequential vertical scan of 20 steps (spaced 150nm), where at each Z-position a measurement was taken for 60 seconds, was then performed in the case of g-GM_1/DiD 2-colour

experiments. For g-Aβ/DiD or g-GM_1/r-Aβ 2-colour experiments, a vertical scan of 15 steps (spaced 200nm) was executed with a 120 seconds measurement time in each step. For FCCS measurements, the membrane was placed on the waist of the focus and data was acquired for a period of 5 min on each GUV.

FLIM-FRET: intensities of the lasers were adjusted at each measurement to avoid pile-up effects (around 1 μW for 470 nm and less than 0.1 μW for 635 nm). An image of 512 × 512 pixels (0.6 ms dwell/pixel) was acquired for each GUV at its cross-section.

Details on analysis of Z-Scan FCS and FLIM-FRET data can be found in **Supplementary notes 1 and 3**.

Molecular Dynamics Simulations: Three membranes with different lipid compositions: DOPC, DOPC/Sph (90/10), and DOPC + GM_1 were investigated. The initial structure of the DOPC bilayer was taken from our previous study [4]. For other membranes a new random configuration was generated with 128 lipids and more than 3 000 water molecules. The initial configuration of the $A\beta_{42}$ peptide was taken from Manna and Mukhopadhyay [5] as the final structure of the simulation, where it interacted with GM_1. $A\beta_{42}$ was investigated to allow the possibility of comparison with previous calculations. All systems were kept electro-neutral and at physiological 150 mM concentration of NaCl. Initial configurations were minimized and then heated to 310 K in 100 ps. The systems were then simulated for at least 1 μs using a 2 fs time step. The bilayers were kept at zero tension with a semi-isotropic pressure coupling at 1 bar using Berendsen barostat [6] with a coupling constant of 2 ps. The system of Aβ peptide in solution what was kept in NpT ensemble with isotropic pressure coupling. The velocity rescale thermostat [7] was employed to keep the temperature at 300 K using 2 ps coupling constant. Short-range interactions were cut off at 1.2 nm, and the effect of long-range Coulomb interactions was accounted for by using the particle mesh Ewald method [8], with a grid spacing of 0.12 nm and cubic interpolation. All bonds were constrained with the LINCS algorithm [9] with the exception of water molecules on which specialized SETTLE algorithm [10] was applied. 3D periodic boundary conditions were used in all simulated systems.

For GM_1 simulation we adapted the system kindly provided by from Manna and Mukhopadhyay [5], where we removed all cholesterol and left only a single GM_1 molecule interacting with the Aβ peptide. The same conformation of the peptide was placed at random positions at pure DOPC membrane and at DOPC membrane with 10 % Sph. Four random positions were generated for the DOPC membrane (simulation a, b, c, d). For the DOPC/Sph (90/10) membrane, ten random positions were generated, out of which four positions were selected (simulation e, f, g, h). Because of the interest in the effect of Sph molecules on the Aβ peptide, the selection was based on the largest number of Sph molecules in the vicinity of the peptide.

All simulations were performed using Gromacs program package version 4.6.6. [11,12] The ffgmx force field was employed for peptide. Berger model was used for lipids [13]. The parameters of sphingomyelin are from Niemelä et al. [14]. Parameters for GM_1 were taken from Sega et al. [15] The SPC model was used for water molecules [16,17]. This set of parameters has been shown to perform well in many membrane simulations [5,17,18].

Supplementary Results.

1 - Characterization of the solutions of Aβ$_{40}$ peptides

To study the membrane-mediated oligomerization of the Aβ$_{40}$ peptide monomers the first concern to address is the characterization of the starting solution of Aβ peptides. Analytical ultracentrifugation of the g-Aβ$_{40}$ peptide in a dilution series was carried out to study whether the peptide is monomeric or might self-assemble to polymeric structures (details in experimental section). The analysis of continuous sedimentation coefficient distributions *c(s)* revealed that the peptide forms only monomeric structure with molecular weights ranging approximately from 4-5 kDa (Supplementary Fig. S1). The peak distribution (narrow peak with no heterogeneity) was negligibly dependent on peptide concentration, which ranged from 1.5 to 4.3 μM. Moreover, Fluorescence Correlation Spectroscopy (FCS) measurements, performed for all prepared Aβ$_{40}$ solutions, report 3D diffusion coefficients (D_{3D}) for Aβ consistent with the expectations for monomeric Aβ peptides. The D_{3D} of r-Aβ in solution were calculated from the 3D diffusion times (τ_{3D}) obtained by FCS measurements (Supplementary Fig. S2). The focal volume waist (ω_0) was estimated by performing FCS measurements of solutions of dyes with known diffusion coefficients. These two parameters were then used to calculate D_{3D} according to the equation

$$D_{3D} = \frac{\omega_0^2}{4\tau_{3D}}$$

The D_{3D} was found to be (1.44±0.08)x10^{-10} m^{2}s^{-1}, which results in a hydrodynamic radius (*rh*) of (1.74±0.09) nm according to the Stokes-Einstein theory. Using the scaling law proposed by Danielsson et al. [19] $\mathrm{rh} = 0.27\mathrm{Mr}^{0.50}$ Å (where M_r is expressed in Da), and $M_r = 5.333 \times 10^3$ Da (Aβ+dye), the monomeric r-Aβ peptide should have an *rh* of 1.97 nm, which is in good agreement with the experimentally determined value.

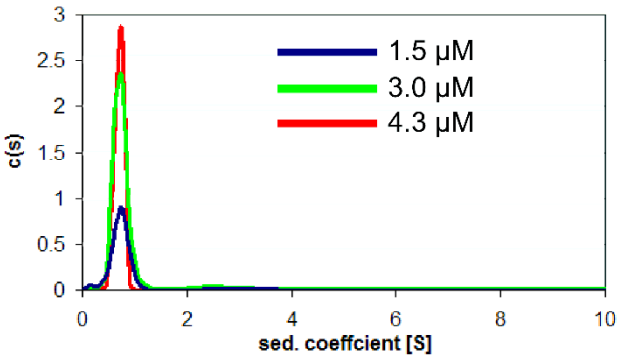

Supplementary Figure S1: Sedimentation coefficient distributions *c(s)*. Obtained with Analytical Ultracentrifugation for g-Aβ solutions of 1.5, 3.0 and 4.3 μM in glucose buffer. Peaks were integrated to determine the weight-averaged sedimentation coefficients s_w.

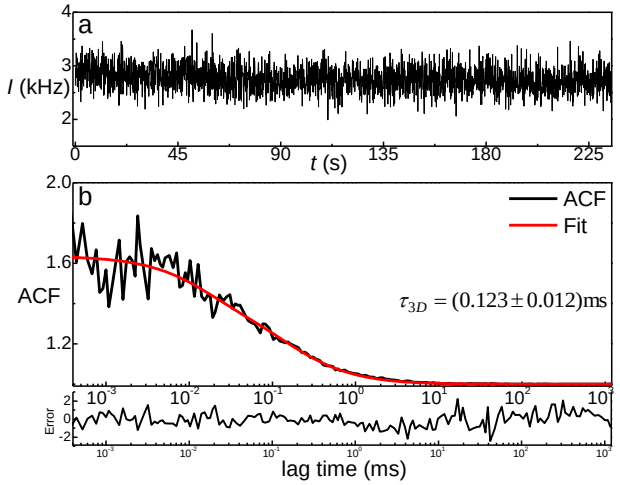

Supplementary Figure S2: Fluorescence Correlation Spectroscopy measurement of Aβ in glucose solution (r-Aβ, 12nM). (**a**) Intensity trace acquired during measurement; (**b**) Autocorrelation function and fit result for 3D diffusion model (error of fit shown below).

Supplementary Results
2 - Supplementary Figures

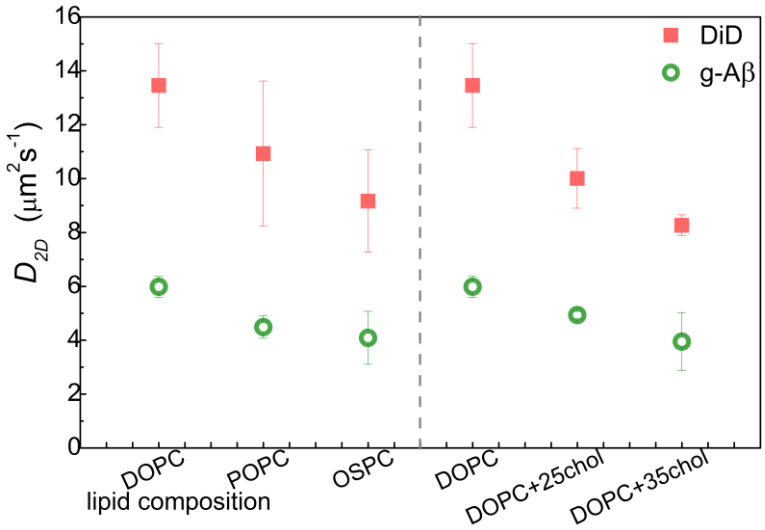

Supplementary Figure S3: Lateral diffusion coefficients, D_{2D}, of membrane bound Aβ (g-Aβ) and lipid tracer DiD in GUVs of different lipid compositions. The lateral diffusion of both g-Aβ and DiD is well described by a one 2D-component model. Values of D_{2D} of Aβ are constant throughout the day of measurements indicating there is no oligomerization of the Aβ peptide. Each point is the weighted average of the D_{2D} results obtained from at least 5 independent 2-coulour Z-scan measurements (each composed of 15 to 20 scans). Error bars represent the standard deviation within the sample of D_{2D} results obtained for each composition.

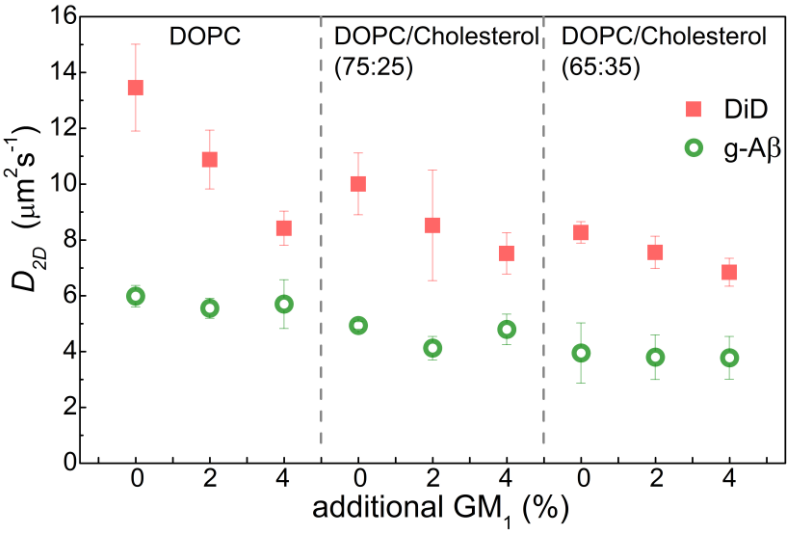

Supplementary Figure S4: Lateral diffusion coefficients, D_{2D}, of membrane bound Aβ (g-Aβ) and lipid tracer DiD in GUVs of different Chol content that contain GM_1 clusters. (**Left panel**) DOPC bilayers containing 0, 2 or 4% GM_1; (**Middle panel**) DOPC/Chol (75/25) bilayers containing 0, 2 or 4% extra GM_1; (**Right panel**) DOPC/Chol (65/35) bilayers containing 0, 2 or 4% extra GM_1. The lateral diffusion of both g-Aβ and DiD is well described by a one 2D-component model. Values of D_{2D} of Aβ are constant throughout the day of measurements indicating there is no oligomerization of the Aβ peptide. Each point is the weighted average of the D_{2D} results obtained from at least 5 independent 2-coulour Z-scan measurements (each composed of 15 to 20 scans). Error bars represent the standard deviation within the sample of D_{2D} results obtained for each composition.

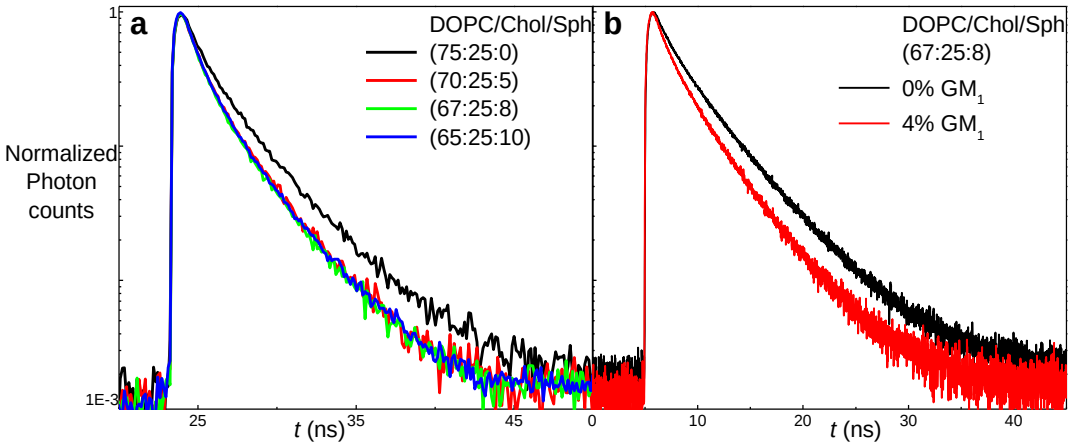

Supplementary Figure S5. Fluorescence decay of donor g-GM$_1$ in FRET experiments using the g-/r-GM$_1$ pair. (a) in DOPC/Chol/Sph bilayers; (**b**) in DOPC/Chol/Sph bilayer with and without the additional 4 mol% of GM$_1$, illustrated example for bilayer containing 8 mol% Sph. The donor decays in all the ternary, and (pseudo)ternary, compositions cannot be fitted with the Baumann-Fayer model. Monte Carlo simulations of the donor decays (note 3: Analysis of FLIM-FRET data) indicate that lateral segregation of the g-/r-GM$_1$ labels must occur. The simulation results show that the segregation within the bilayer occurs at the nanoscale. The simulations allow to characterize the radius and area coverage of the nano-heterogeneities, or nanodomains, which are reported in Table 1 within the main text of the manuscript (for more details, see note 3: analysis of FLIM-FRET data).

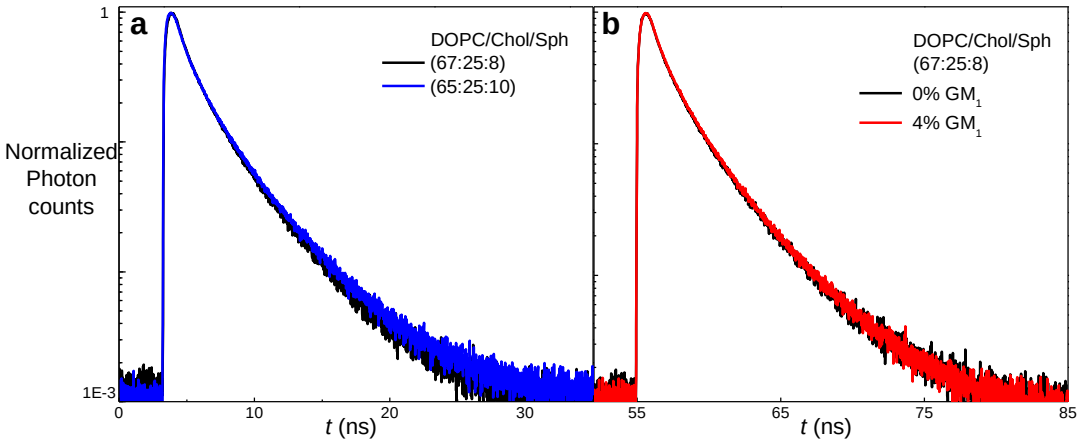

Supplementary Figure S6. Fluorescence decay of donor g-GM$_1$ in FRET experiments using the g-GM$_1$/DiD pair.(**a**) in DOPC/Chol/Sph bilayers; illustrated for 8 mol% and 10 mol% of Sph,(**b**) in DOPC/Chol/Sph bilayer with and without the additional 4 mol% of GM$_1$, illustrated example for bilayer containing 8 mol% Sph. With this donor/acceptor pair, the donor decays remain unaltered in all the studied lipid bilayers. This implies that the acceptor is neither preferentially segregated from the donor nor preferentially co-localizing with the donor. The FRET data indicate that the acceptor DiD is homogenously distributed within the bilayers of all the compositions presented in this manuscript, even in the presence of the GM$_1$ nanodomains.

Supplementary Results.
3 - All-atom molecular dynamics simulations

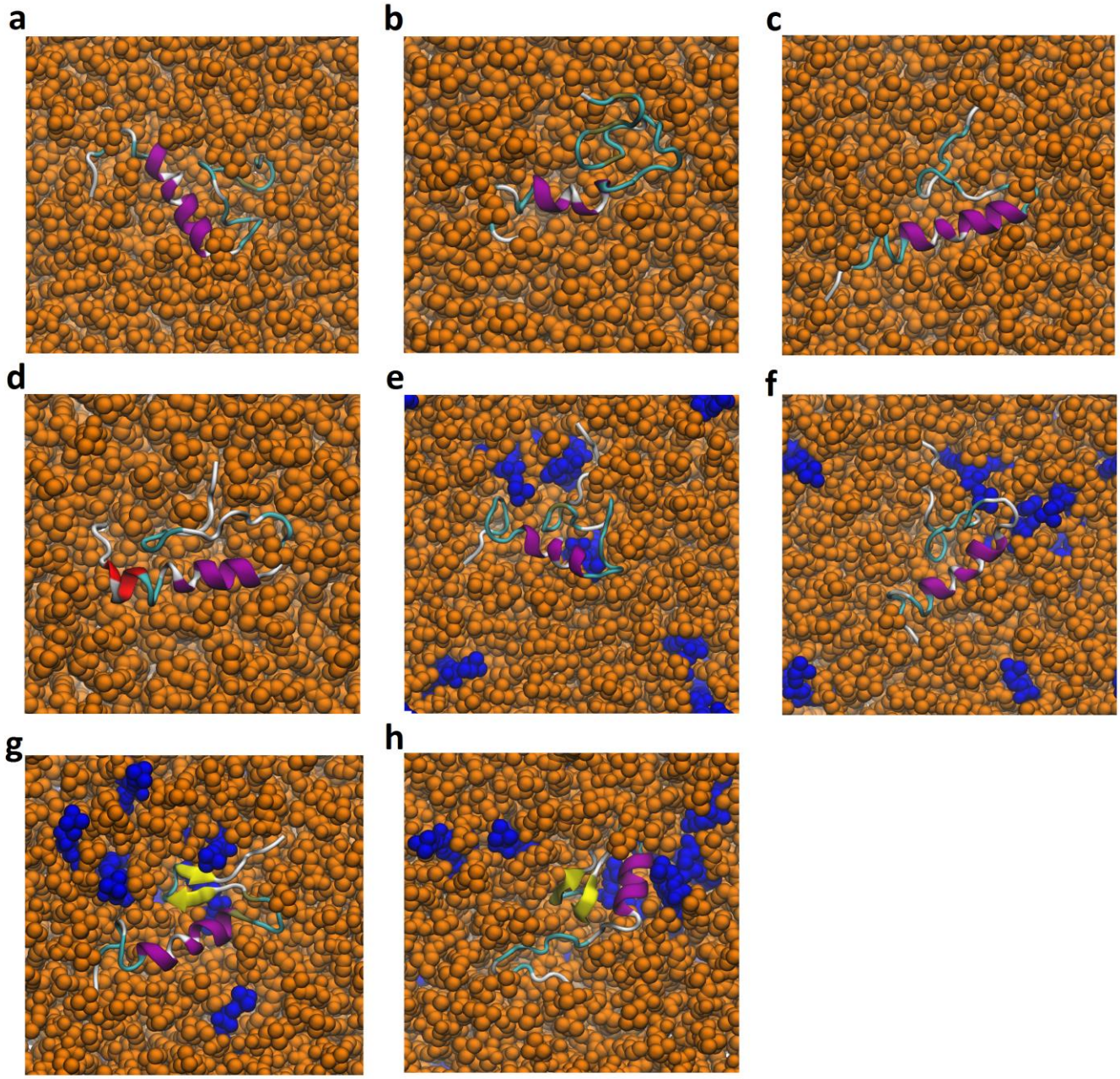

Supplementary Figure S7. Top view snapshots of Aβ peptide interacting with the lipid membranes. (**a-d**) DOPC membrane. (**e-h**) DOCP membrane with 10% sphingomyelin. Snapshots are taken at the end of the 1.5 μs simulation. Color-coding: DOPC – orange; Sphingomyelin – blue; Aβ peptide – new cartoon visualization with coloring based on the secondary structure (alpha helix – purple, pi-helix – red, beta sheet – yellow, coil – white, turn - cyan).

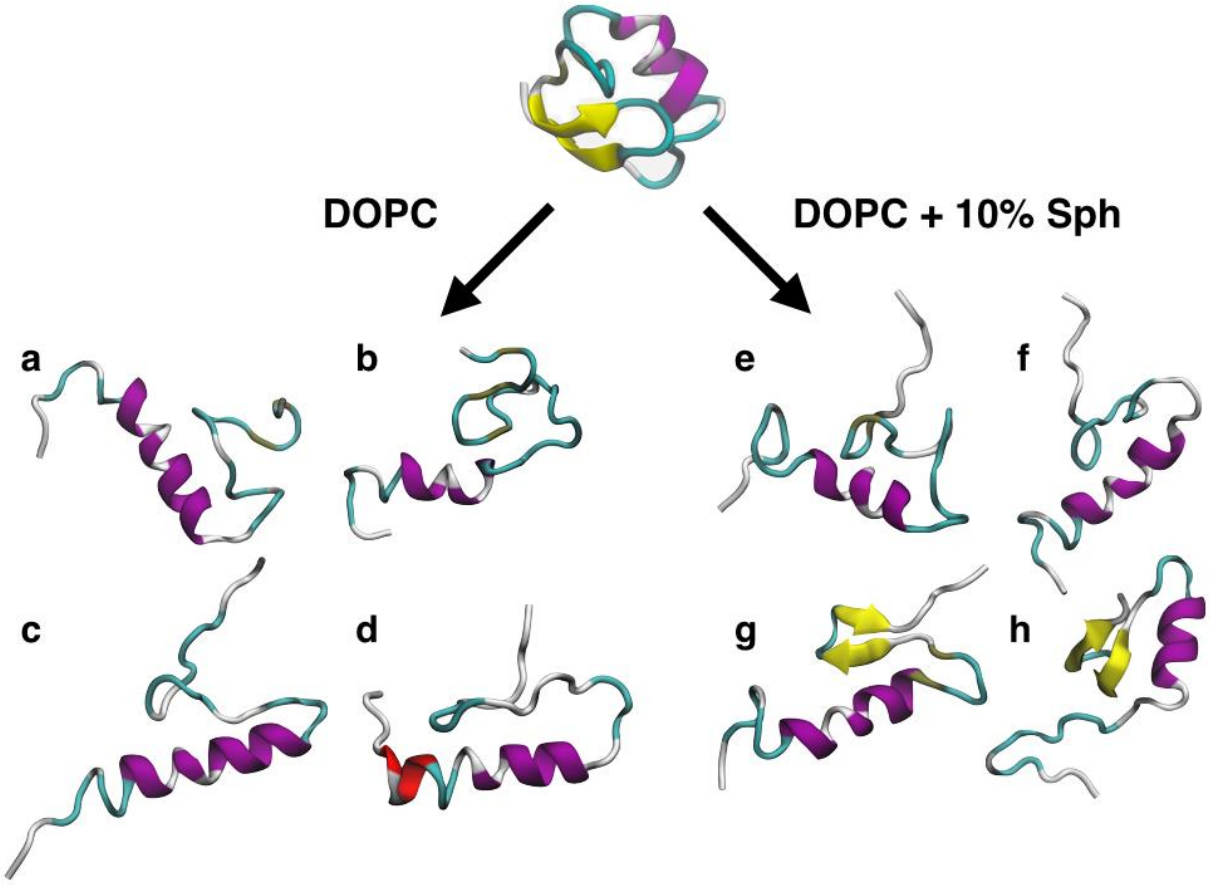

Supplementary Figure S8. Final configurations of Aβ peptide in 9 independent simulations of 1.5 μs. Top: Aβ in solution; **a-d**) Aβ in pure DOPC bilayer; **e-h**) Aβ in DOPC/Sph (90/10) membrane, where the peptide was in contact with Sph.

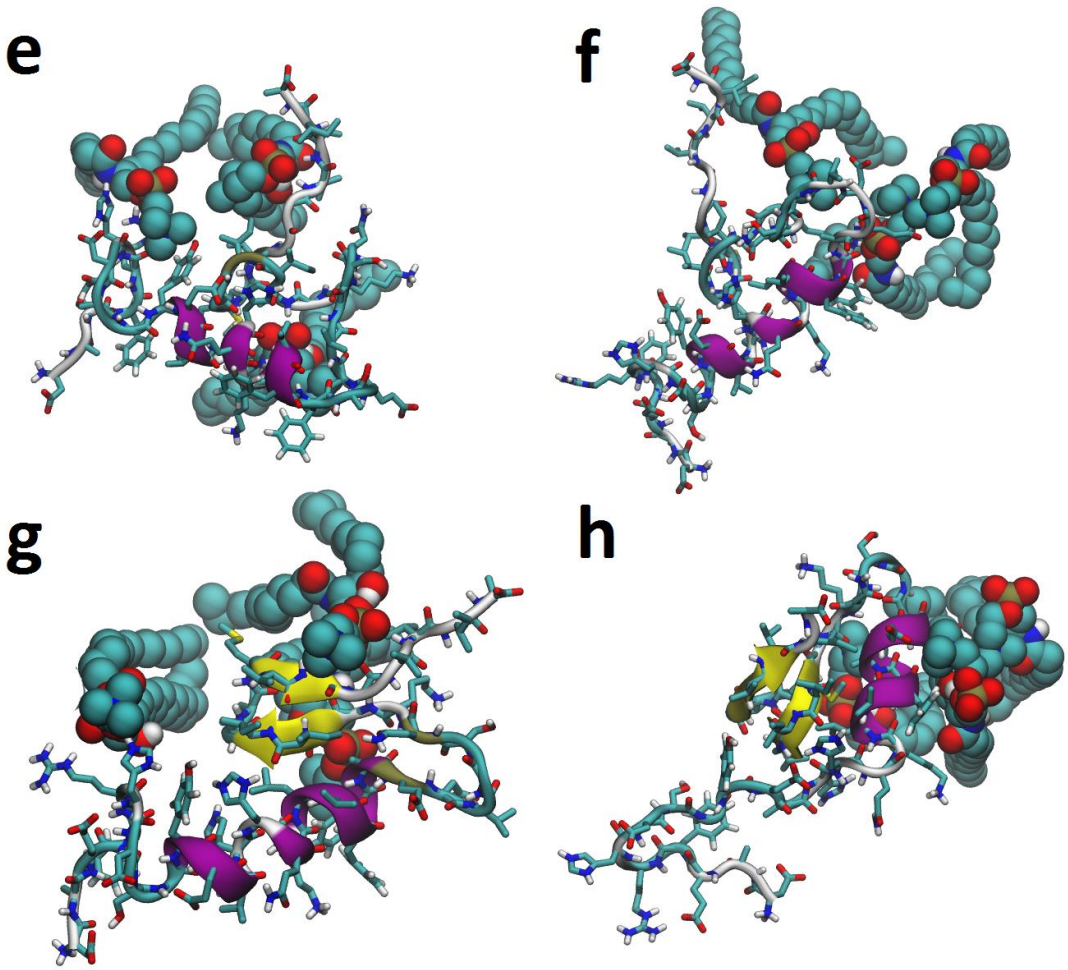

Supplementary Figure S9. Detailed snapshots of the Aβ peptide interacting with sphingomyelin lipids. (**e-h**) DOCP membrane with 10% sphingomyelin. Snapshots are taken at the end of the 1.5 μs simulation. Aβ peptide shown with new cartoon visualization (color-code based on the secondary structure: alpha helix – purple, pi-helix – red, beta sheet – yellow, coil – white, turn - cyan) and explicit residues. Sphingomyelin atoms are represented as solid van der Waal spheres. The amino acids of the Aβ peptide interacting with sphingomyelin are as follows: (**e**) ARG5, HIS6, TYR10, HIS13, ALA30, MET35, GLY38, VAL39, VAL40; (**f**) PHE20, GLU22, ASP23, VAL24, GLY25, LYS28, VAL40, ILE41; (**g**) ARG5, HIS6, PHE20, GLY29, LEU34, MET35, ALA36, GLY37, GLY38, VAL39, VAL40; (**h**) LYS16, PHE19, PHE20, GLU22, ASP23, VAL24, LYS28, MET35. Interestingly, the peptides with β-sheet structure did not show hydrogen bonds with NH or OH groups of Sph. Therefore, one cannot simply attribute the induction of conformational change by Sph to an interaction between the peptide and atomic groups unique to Sph.

The radius of gyration, total amount of secondary structure, and hydrophobic and hydrophilic areas of the peptide exposed to solvent were similar in both DOPC and DOPC/Sph membranes (Figures S10 to S13)

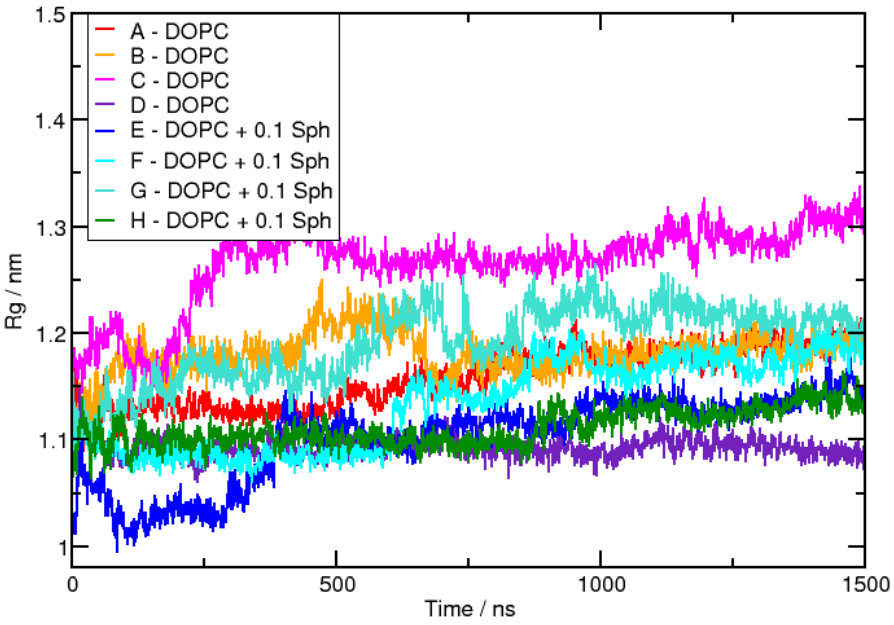

Supplementary Figure S10. Development of the radius of gyration of Aβ peptide. Results are shown for the total 1.5 μs of the simulations. (**a-d**) DOPC membrane. (**e-h**) DOCP membrane with 10% sphingomyelin.

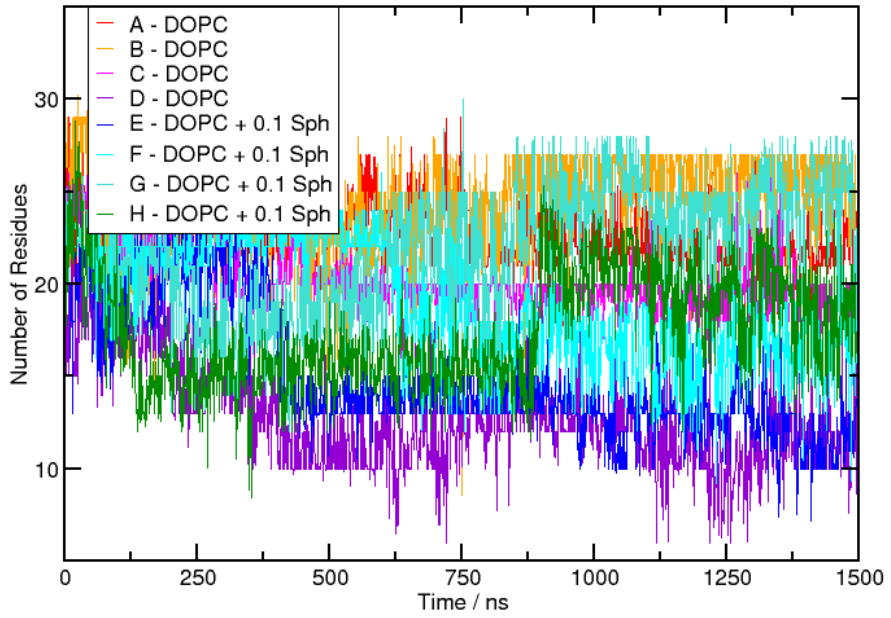

Supplementary Figure S11. Development of the total amount of secondary structure of Aβ peptide. Results are shown for the total 1.5 μs of the simulations. (**a-d**) DOPC membrane. (**e-h**) DOCP membrane with 10% sphingomyelin.

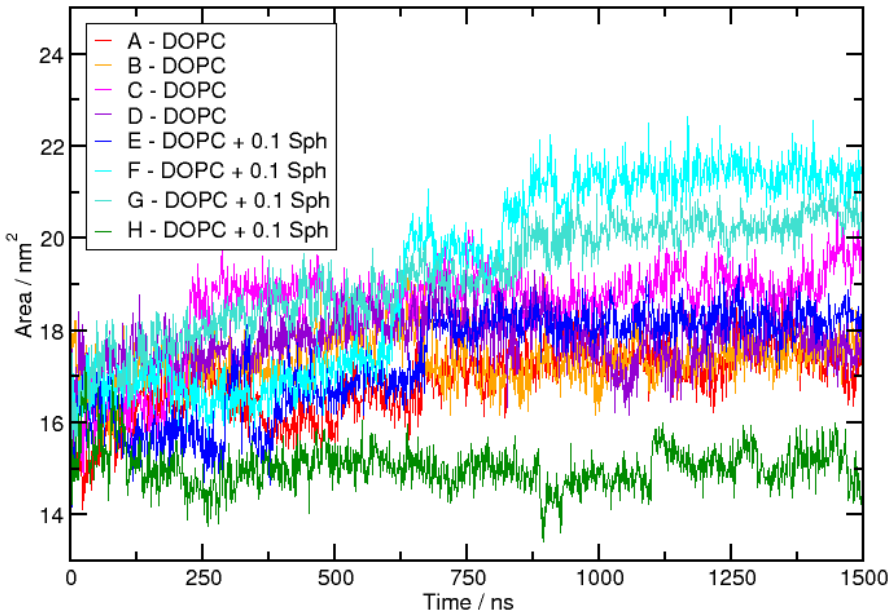

Supplementary Figure S12. Development of the total hydrophobic area of the Aβ peptide that is exposed to solvent. Results are shown for the total 1.5 μs of the simulations. (**a-d**) DOPC membrane. (**e-h**) DOCP membrane with 10% sphingomyelin.

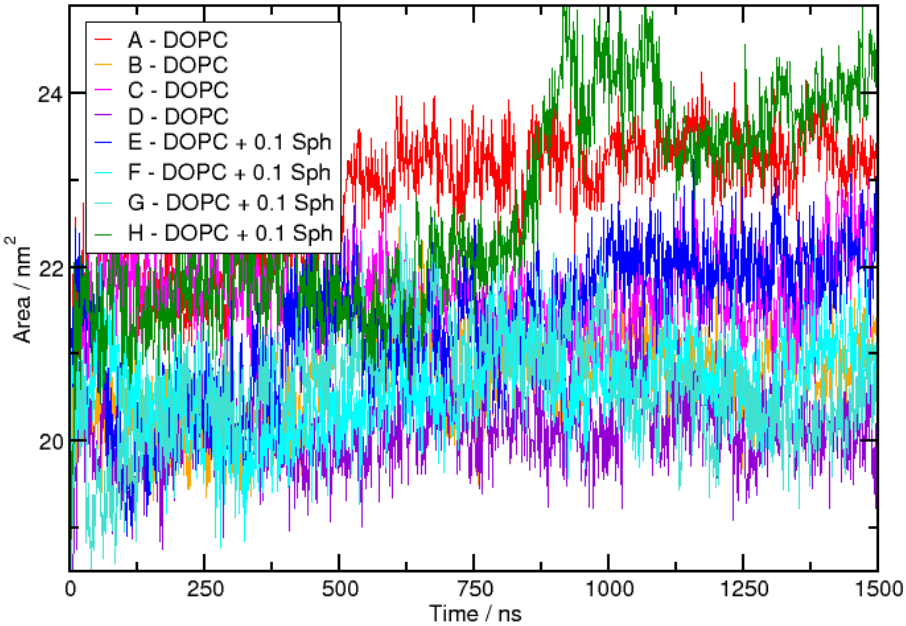

Supplementary Figure S13. Development of the total hydrophilic area of the Aβ peptide that is exposed to solvent. Results are shown for the total 1.5 μs of the simulations. (**a-d**) DOPC membrane. (**e-h**) DOCP membrane with 10% sphingomyelin

Supplementary Figure S14. Development of the secondary structure of the Aβ peptide. (**a-d**) DOPC membrane. (**e-h**) DOCP/Sph (90/10) membrane. Results are shown for the total 1.5 μs of the simulations. Color code: **cyan**= turn; **yellow** = beta-sheet; **dark yellow** = isolated bridge; **pink** = alpha helix; **blue** = s-10 helix; **red** = pi helix; **white** = coil.

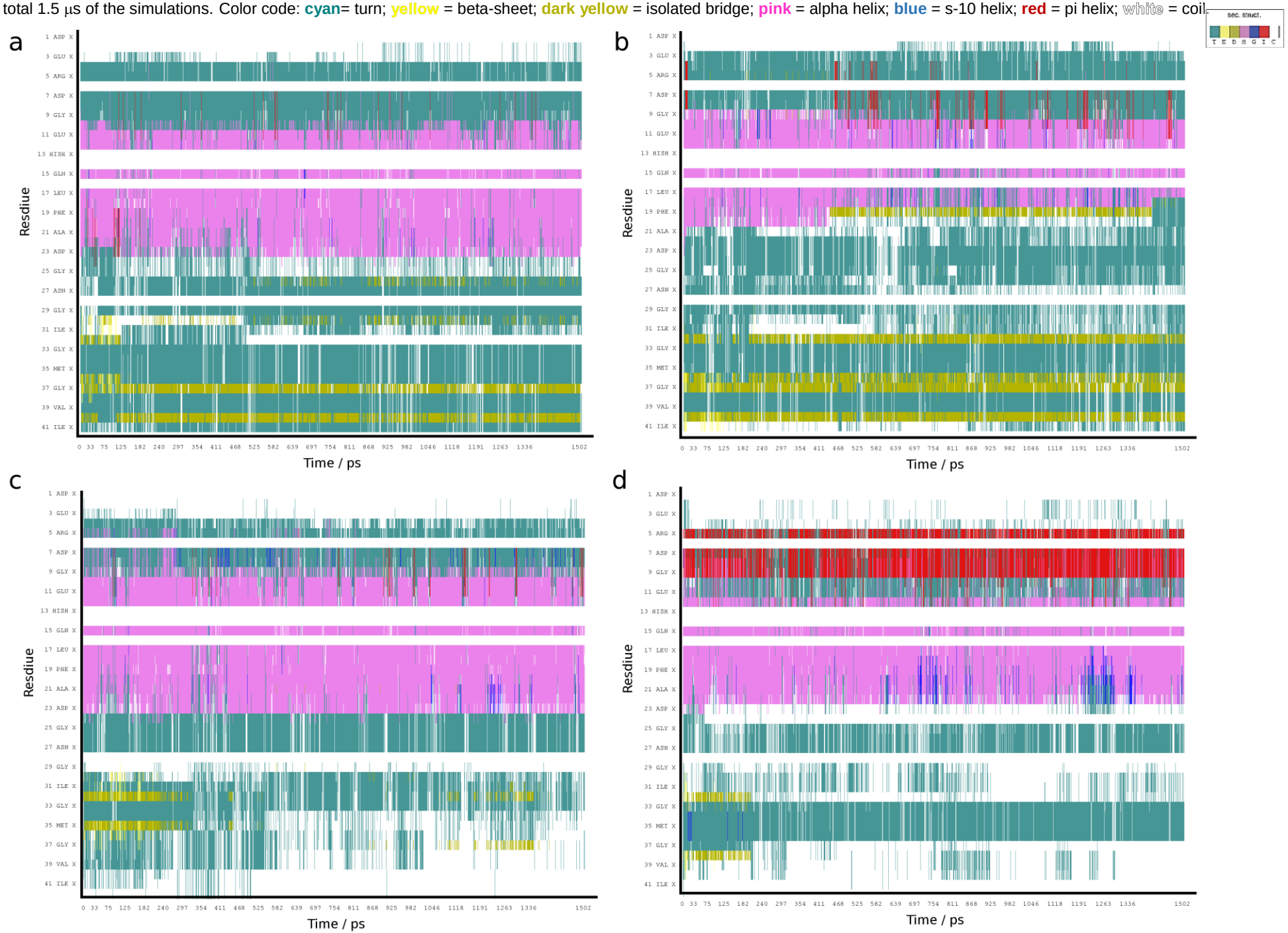

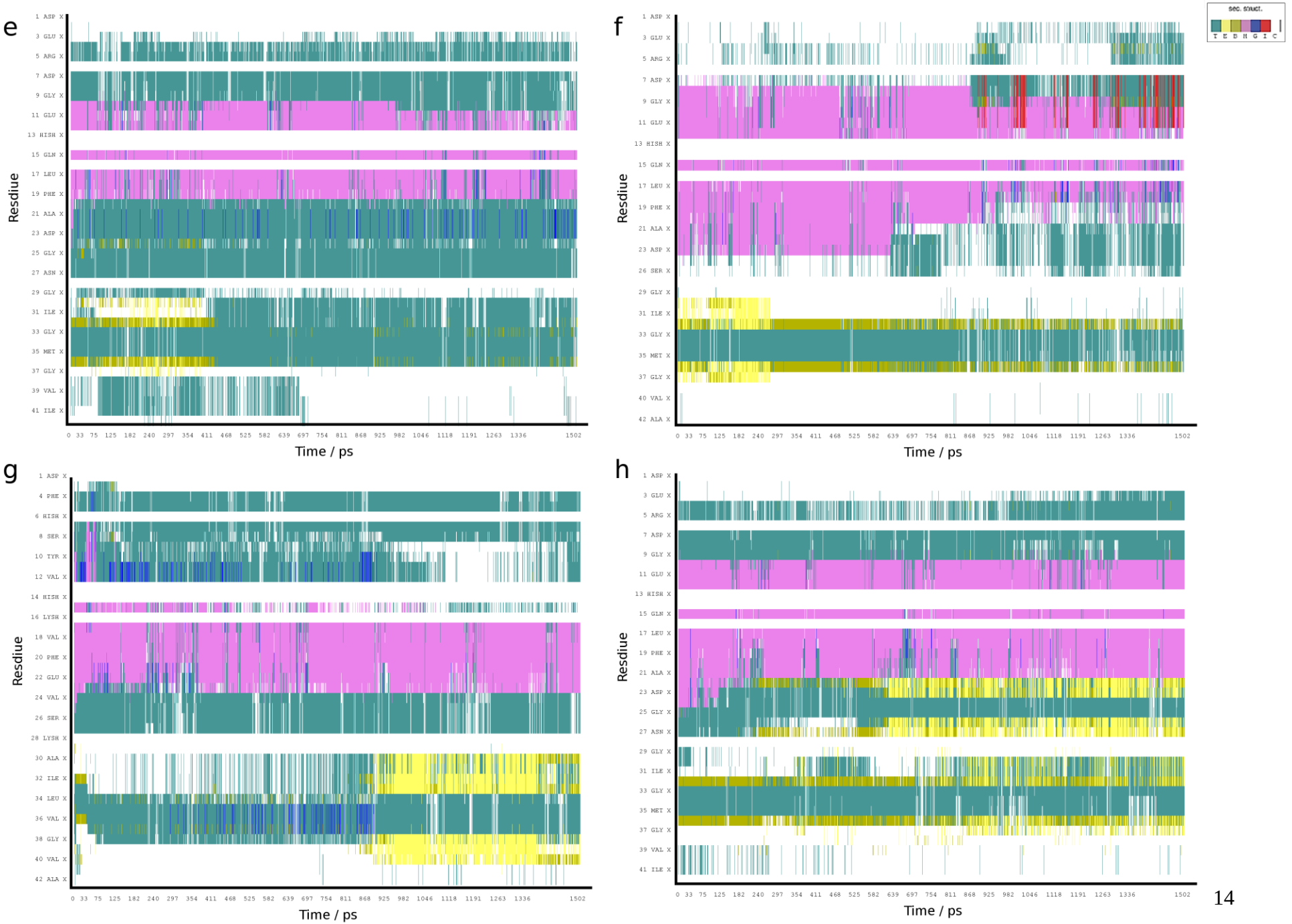
e
f
g
h
Resdiue
Time / ps
Sec. Struct.
T E B H G I C
0 33 75 125 182 240 297 354 411 468 525 582 639 697 754 811 868 925 982 1046 1118 1191 1263 1336 1502

Supplementary Figure S15. Development of the secondary structure of the Aβ peptide. The final Aβ peptide conformations containing the beta-sheet structure at the C-terminal obtained in the membrane with Sph (simulation g and h) were transfered to a pure DOPC membrane to test the stability of the obtained beta-sheet conformation. First the peptide was inserted and well equilibrated in DOPC bilayer while the conformation was constrained and only then the unconstrained simulation was started with the freely moving peptide. The beta-sheets were found to fully or partially unfold within 1 μs when in the pure DOPC membrane, supporting the finding that the beta-sheet is induced by the presence of Sph. (**Top**) figures show the initial and final conformation of the peptide (**top left** – initial structure from simulation g; **top right** – initial structure from simulation h). (**Bottom**) figures show the corresponding development of the secondary structure of the Aβ peptide once put in the pure DOPC membrane. Color code: **cyan**= turn; **yellow** = beta-sheet; **dark yellow** = isolated bridge; **pink** = alpha helix; **blue** = s-10 helix; **red** = pi helix; white = coil.

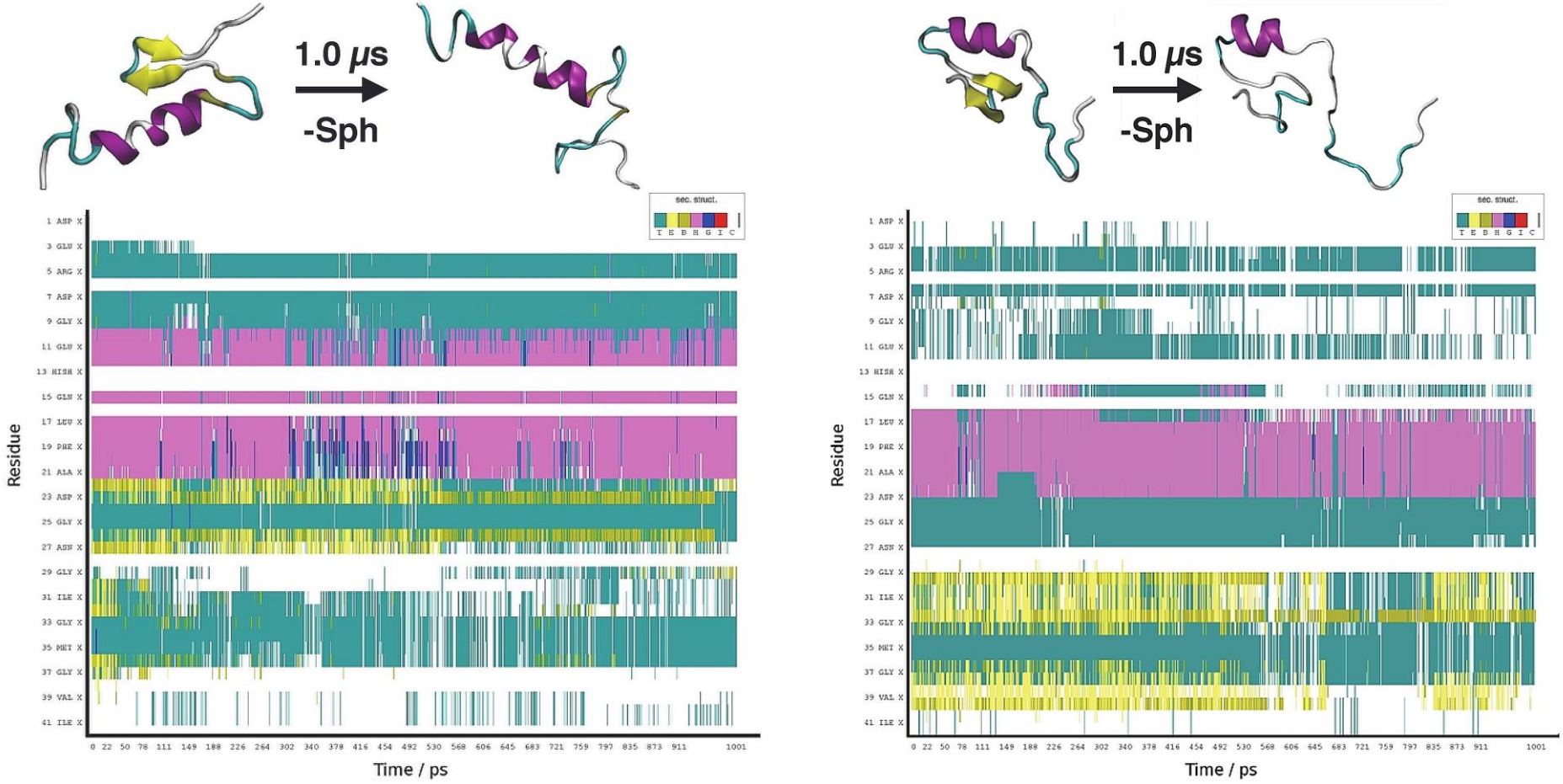

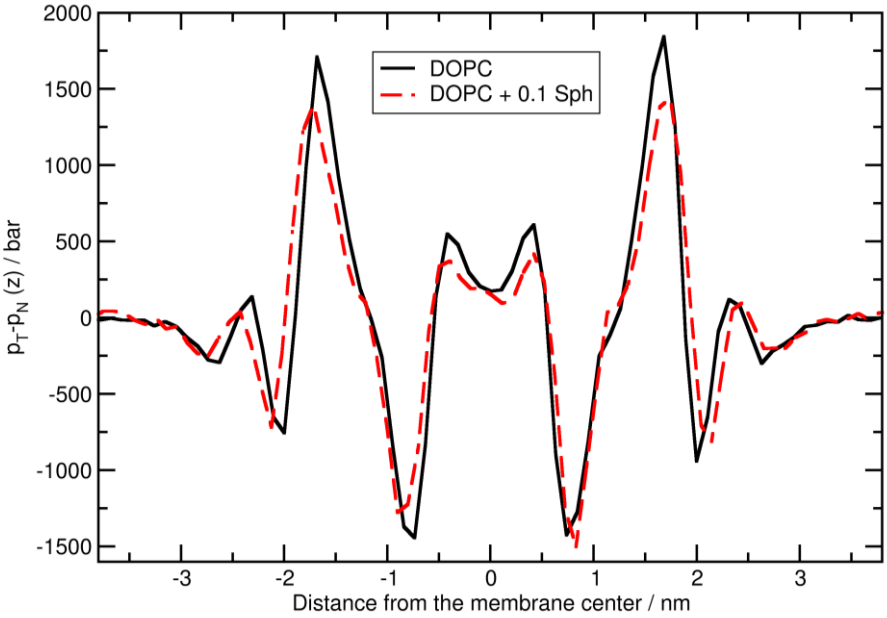

Supplementary Figure S16. Lateral pressure profiles. (**black**) pure DOPC membrane; (**red**) DOCP membrane with 10% sphingomyelin. The presence of Sph altered membrane lateral pressure profile compared to the pure DOPC membrane

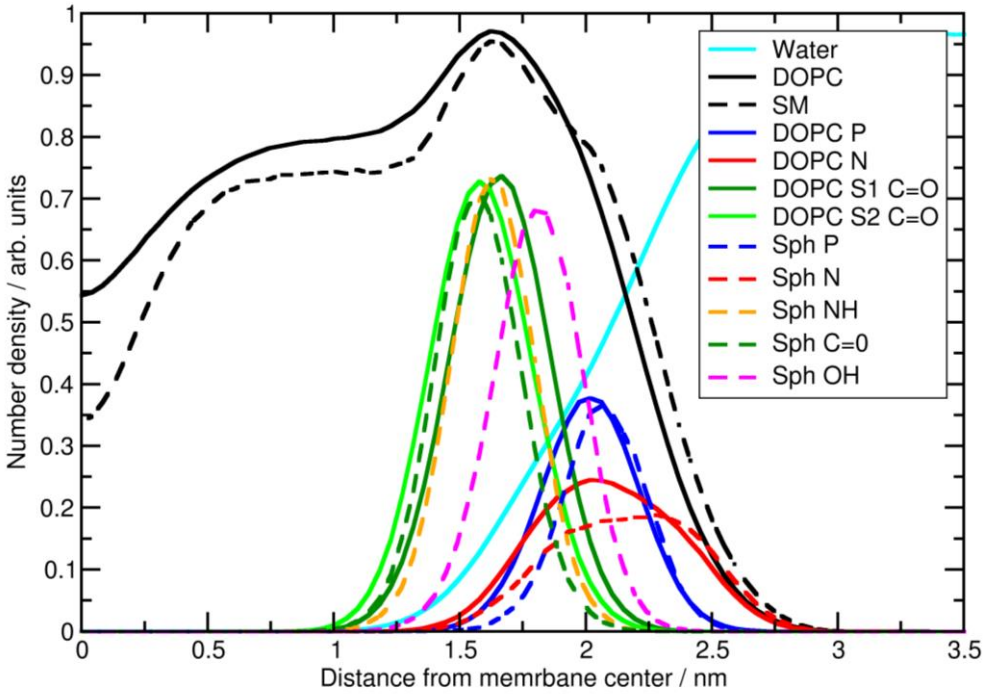

Supplementary Figure S17. Partial density profiles of DOPC membrane with 10% sphingomyelin. Data corresponding to DOPC molecules are represented by full line, data corresponding to the Sphingomyelin (Sph) molecules is represented by dashed line. Data is an average over 100ns. The phosphocholine headgroup of Sph is moved out of the membrane when compared to the phosphocholine headgroup of DOPC. Below the headgroups, the carbonyl of Sph resides deeper within the membrane when compared to the carbonyl of DOPC. The overall density profile of Sph is also quite different from that of DOPC.

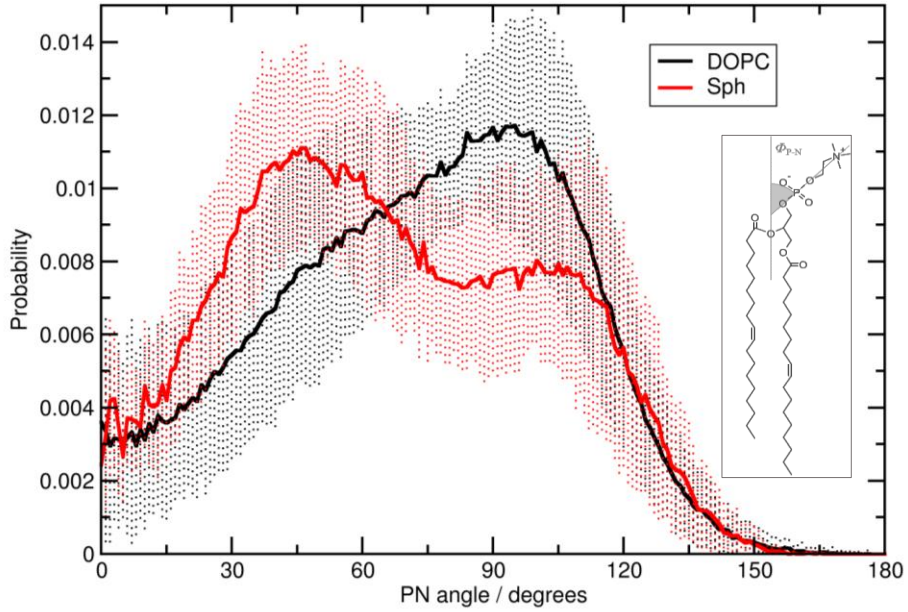

Supplementary Figure S18. Distribution of the angles between the P-N dipole and the membrane normal. (**black**) DOPC; (**red**) sphingomyelin. Obtained from the simulations of the DOPC membrane with 10% of sphingomyelin and averaged over 100 ns of the simulation. Dots depicts the standard deviation. **Inset**: chemical structure of DOPC showing the definition of the PN angle. The phosphocholine headgroup orientation is different for Sph compared to DOPC. The headgroups of Sph exist in two distinct populations, displaying on average a more perpendicular orientation to the membrane plane compared to DOPC. This is due to hydrogen bond formation between the hydroxyl group and phosphate oxygens at the headgroup of Sph (see below Figure S19), which is in agreement with previous simulations employing different parameterizations.[20,21]

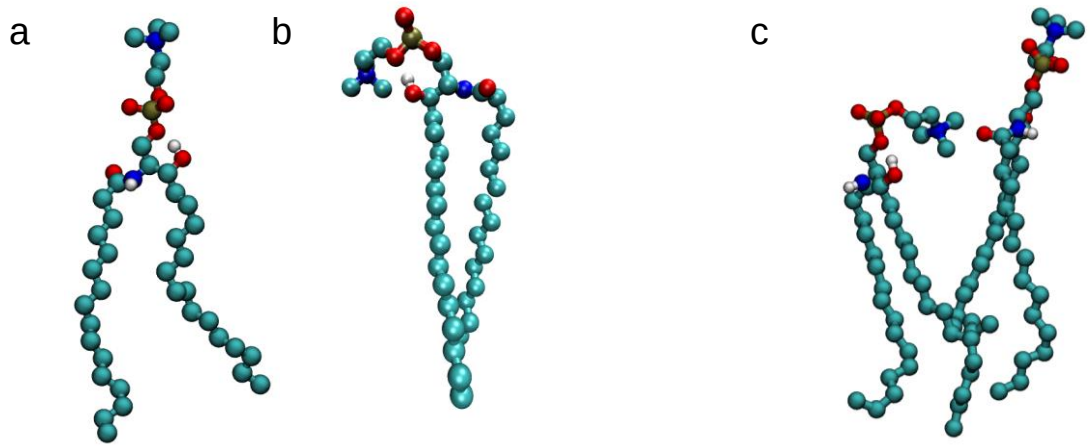

Supplementary Figure S19. Illustrative snapshots of the common configurations of Sphingomyelin that illustrate the effects of hydrogen bonds. (**a-b**) two possible configurations for isolated molecules; (**c**) configuration of a sphingomyelin pair. The hydroxyl group forms a hydrogen bond with the phosphate oxygens. When in pairs, sphingomyelin was found with a tilted orientation of its headgroup where the choline group was interacting with the carbonyl group of the neighbouring molecule.

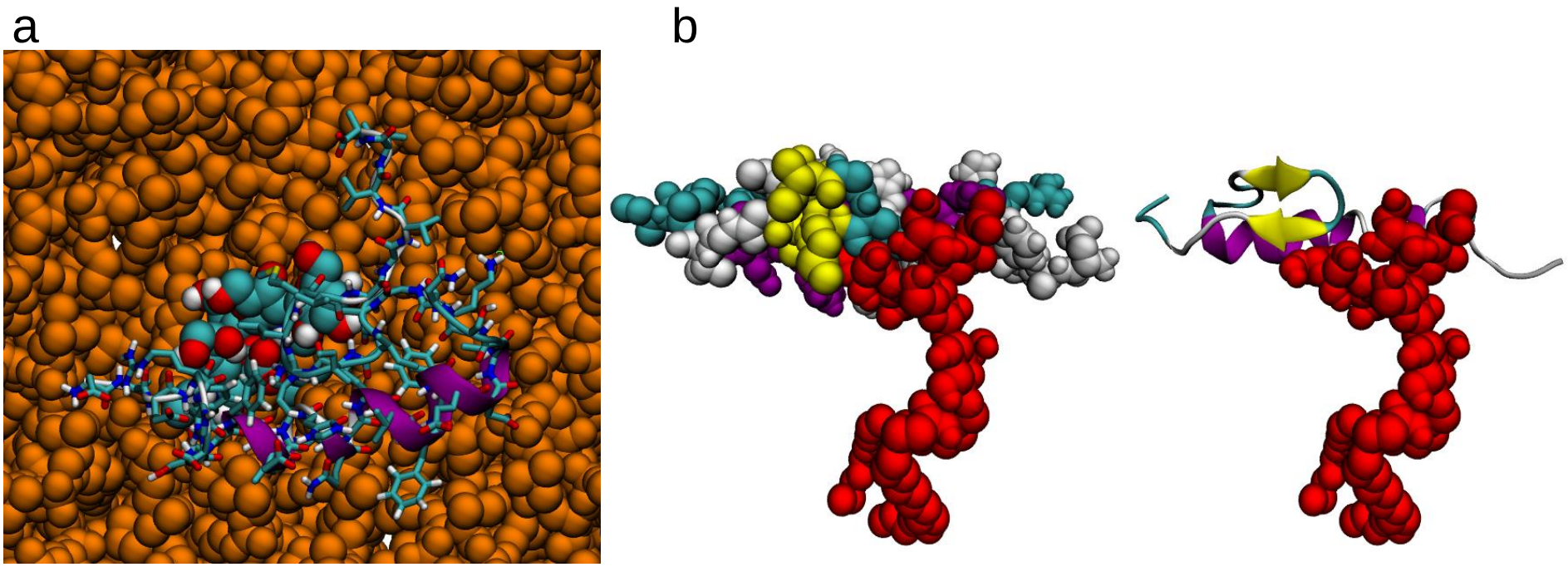

Supplementary Figure S20. Snapshot of the Aβ peptide interacting with GM_1. a) Top view. Aβ peptide shown with new cartoon visualization and explicit residues. GM_1 atoms are represented as solid van der Waal spheres. DOPC molecules are shown in orange as solid van der Waal spheres. **b**) Side view. GM1 atoms are represented as red solid van der Waal spheres. Aβ peptide shown as solid van der Waal spheres (**left**) or new cartoon visualization (**right**), color-code based on the secondary structure: alpha helix – purple, pi-helix – red, beta sheet – yellow, coil – white, turn - cyan). Our simulation with GM_1 demonstrated strong interaction between Aβ peptide and GM_1, in aggreament with previous findings [5]. The Aβ peptide was interacting with GM_1 via the amino acids PHE4, HIS13, LYS16, LEU 17, LEU34, MET35, VAL36. The peptide is restricted by the specific interaction with GM_1, contrary to what is found in the DOPC/Sph simulation where no specific bonding was observed. Significantly, the Aβ remained bound to GM_1 within the whole 1μs simulation. The C-terminus of the peptide maintained a β-sheet conformation in similarity to when it was bound to a GM_1 cluster.[5] The β-sheet forming residues of Aβ were an integral part of the contacts with GM_1.

Supplementary Note 1
Analysis of Z-FCS data

Z-scan Fluorescence Correlation Spectroscopy (Z-FCS) is a technique for obtaining absolute diffusion coefficients that overcomes the positioning and calibration problems associated with FCS measurements in planar systems [22,23]. Z-FCS also resolves simultaneous two- and three-dimensional diffusion and allows the determination of diffusion laws [24]. The technique is based on measuring fluorescence Autocorrelation Functions (ACF) at well-defined positions along the optical axis of the microscope (the Z axis). The distance Δ_z between the sample and the waist of the focus is changed in steps typically of 100 to 200 nm. The measured lateral diffusion time (τ_{2D}) and particle number (*N*) parameters follow a parabolic dependence with Δ_z. This allows for the determination of the lateral diffusion coefficient (D_{2D}) as well as surface concentration of the diffusing fluorescent particles.

The ACF acquired by Z-FCS were fitted to diffusion models in order to recover the 2D diffusion coefficients, D_{2D}. Each of the ACF acquired at the different positions during the Z-scan was fitted individually. The ACF (G_τ) for the lipid tracer DiD and the labeled GM_1 molecule were fitted with a model for Brownian diffusion in a two-dimensional surface considering fluctuations caused by the photophysical characteristics of the dye (i.e. triplet state formation) [24]:

$$G_\tau = 1 + [1 - T + T\ exp(-\tau/\tau_T)]\frac{1}{N(1-T)}\frac{1}{1+(\tau/\tau_D)}$$

where τ_D is the diffusion time of the molecule, *N* is the particle number, and *T* and τ_T characterize the contribution and kinetics of triplet state, respectively.

The ACF for the g-/r-Aβ peptides were fitted to a model containing contributions from both two- and three-dimensional diffusion to account for the fraction of the Aβ peptides that remained in solution, unbound to the lipid membrane [24]:

$$G_\tau = 1 + [1 - T + T\ exp(-\tau/\tau_T)]\frac{1}{N(1-T)} \times \left[\frac{(1-F_{2D})}{1+(\tau/\tau_{3D})}\frac{1}{[1+(\tau/\tau_{3D})(w_0/w_z)^2]^{\frac{1}{2}}} + \frac{F_{2D}}{1+(\tau/\tau_{2D})}\right]$$

where τ_{2D} and τ_{3D} are the diffusion times of the molecules diffusing in two and three dimensions, respectively; w_0 and w_z are characteristic parameters of the detection volume; and F_{2D} is the fraction of bound (2D) molecules within the particle number *N*. τ_{3D} was determined by FCS measurements in the bulk solution surrounding the GUVs for each and every sample prepared. The value was introduced as a fixed parameter in the fitting routine.

The above models, where the anomalous exponent α is equal to 1, yielded good fit results for all the ACF of the several molecules. The anomalous exponent is included in a model of the ACF, where the term (τ/τ_{2D}) is replaced by $(\tau/\tau_{2D})^\alpha$, in order to describe anomalous diffusion. For our data, there was no need to adjust the α parameter to values different than 1 which indicates that the diffusion of the molecules within the bilayer is consistent with unhindered motion. However, the FCS data for the Aβ peptides is noisy and such quality does not allow to exclude the possibility of hindered Aβ diffusion.

The resulting g τ_{2D} and *N* values vary with the z-position of the focus [22], which allows for the determination of the lateral diffusion coefficient D_{2D}. The dependence of τ_{2D} can be described by [22]:

$$\tau_{2D} = \frac{w_0^2}{4D_{2D}}\left(1 + \frac{\lambda^2\Delta_z^2}{\pi^2 n^2 w_0^4}\right)$$

where *n* is the refractive index, λ is the excitation wavelength and Δ_z the distance between the sample position and the position of the beam diameter minimum.

Z-FCS acquires the ACF over several different sizes of detection areas. This inherent feature of the scan allows to measure the so-called diffusion law. The linear dependence of τ_{2D} on N/N_0, for each Δ_z, is given by [24]

$$\tau_{2D} = t_0 + \frac{w_0^2}{4D_{\text{eff}}}\frac{N}{N_0}$$

where D_{eff} is the effective diffusion coefficient and N_0 is the particle number in the waist of the focus. Z-FCS can, therefore, distinguish the diffusion regime and provide information on membrane structure.

The diffusion laws obtained for all fluorescently labeled lipid molecules (DiD and g-/r-GM_1) showed no evidence of hindered diffusion in all the lipid system investigated.

Supplementary Note 2
Phase diagrams

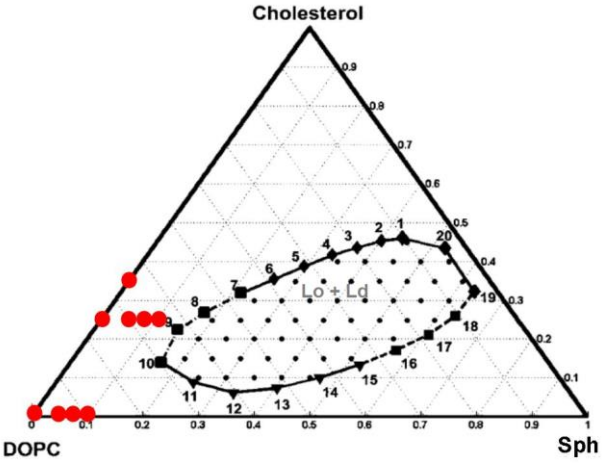

Supplementary Figure S21. Ternary phase diagram for DOPC/Chol/Sph lipid mixtures. Adapted from Smith and Freed[25]. The dotted area of the diagram represents the Ld/Lo phase coexistence region. The red dots represent the DOPC/Chol/Sph lipid compositions used in this study. The (pseudo)ternary mixtures, with the extra GM_1 component, were based on the same lipid compositions. The GM_1 content is 2-4 mol% of total (DOPC/Chol/Sph) lipids, detailed compositions are given in note 4 of the Supplementary Information.

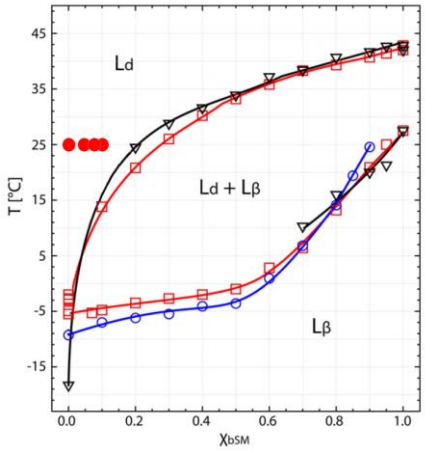

Supplementary Figure S22. Binary phase diagram for DOPC/Sph lipid mixtures. Adapted from Petruzielo et al.[26]. Onset and completion temperatures for DOPC/Sph are represented by the black triangles. The red dots represent the DOPC/Sph lipid compositions used in this study.

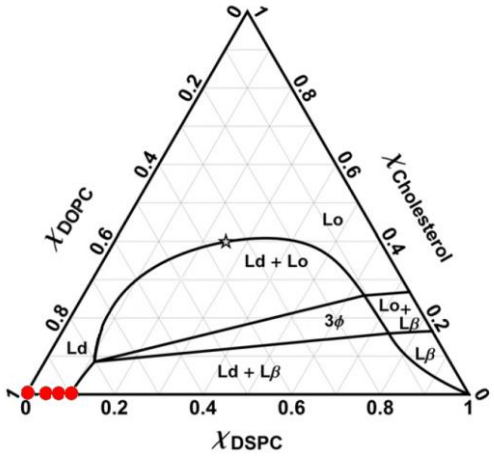

Supplementary Figure S23. Ternary phase diagram for DOPC/Chol/DSPC lipid mixtures. Adapted from Heberle et al.[27]. The red dots represent the DOPC/DSPC lipid compositions used in this study.

Supplementary Note 3
Analysis of FLIM-FRET data

In Fluorescence Lifetime Förster Resonance Energy Transfer (FLIM-FRET), the Förster resonance energy transfer (FRET) efficiency is obtained from Fluorescence Lifetime Images (FLIM). In such images each pixel contains information on the arrival times of the detected individual photons. The arrival times are used to construct a histogram, i.e. the fluorescence decay. The decay can then be analyzed with an appropriate mathematical model that accounts for FRET.

Analytical equations describing FRET exist for the case of donors (*D*) and acceptors (*A*) distributed uniformly in several parallel planes of a lipid bilayer. Such situation has relevance in this work in the case of the randomly distributed lipid tracer DiD and GM_1 probes, and can be described by the Baumann-Fayer model [28]. Complex analytical models must be derived for other specific system topologies. Here, it is assumed that the dynamic limit conditions are fulfilled as *D* and *A* are localized at the lipid water interface. FRET occurring within one bilayer leaflet is named *intra*-FRET and the *D* survival probability function $G_{intra}(t)$, can be expressed as [28]

$$ln\, G_{intra}(t) = -C_2 \Gamma\left(\frac{2}{3}\right)\left(\frac{t}{\tau}\right)^{1/3}$$

where C_2 is the reduced surface concentration of acceptors, which represents the average number of *A* surrounding the *D* within an area πR_0^2, Γ is the gamma function and τ is the average lifetime of the donor. FRET occurring between two parallel leaflets of the lipid bilayer that are separated by the distance *d* is named *inter*-FRET and the *D* survival probability function $G_{inter}(t)$, can be expressed as [28]

$$ln\, G_{inter}(t) = -\frac{C_2}{3}\left(\frac{d}{R_0}\right)^2\left(\frac{2\mu}{3}\right)^{1/3}\int_0^{2/3\mu}(1-e^{-s})s^{-4/3}ds$$

where θ_r is the angle between the bilayer normal and the vector connecting the locations of the donor and acceptor dipoles, $\mu = 3t\left(\frac{R_0}{d}\right)^6\frac{1}{2\tau}$ and $s = 2\mu\cos^6\frac{\theta_r}{3}$. Both *inter*- and *intra*-FRET may occur simultaneously in a lipid bilayer. Therefore, the total survival probability of *D* is given by the joint probability $G(t) = G_{\text{intra}}(t)G_{\text{inter}}(t)$ and the fluorescence intensity $F(t)$ of a *D* in the presence of *A* decays according to

$$F(t) = G(t)\sum_i \alpha_i\, exp\left(-\frac{t}{\tau_i}\right)$$

where $\sum_i \alpha_i\, exp(-t/\tau_i)$represents the decay of a *D* in the absence of FRET. The acceptor surface concentration C_2 and the bilayer thickness *d* have been determined by this model and used for domain size determination.

Domain size determination is performed by Monte Carlo simulations where FRET across the phase separation boundary is considered, on the contrary to other procedures [29]. The process consists of generating a simulated decay of *D* undergoing FRET. A number of *D*, *A* and circular domains with a defined radius are generated on the bilayer surface. *D* and *A* are distributed according to the distribution constants defined as $K_D = [D_{\text{inside}}]/[D_{\text{outside}}]$, $K_A = [A_{\text{inside}}]/[A_{\text{outside}}]$.This is followed by random excitation of a *D* and calculation of the time when a FRET event takes place. This is a random process that is modulated by the overall energy transfer rate Ω_i according to $\Delta t_i = -\ln\gamma/\Omega_i$ where γ is a randomly generated number between 0-1. The outcome of each simulation step is the time interval Δt_i between the excitation and FRET event. For good statistics, each generated step is used approximately 100 times before a new one is generated and the total number of excitation events is usually higher than $3x10^5$. By constructing a histogram of Δt_i intervals the total survival probability function $G(t)$ is obtained and the simulated decay of donors undergoing FRET calculated. The simulated decay is matched to the experimental one by varying the domain radius and the number of domains.

Further considerations

In the simpler lipid compositions (DOPC, POPC, OSPC, DOPC/Chol) without the additional (unlabeled) GM_1, fitting of the *D* decays to the Baumann-Fayer model yields C2 and d parameters that are in good agreement with a priori known surface concentration and the bilayer thickness. From this, one can conclude that the labeled GM_1 molecules used as the FRET pair (g-GM_1 and r-GM_1) are homogeneously distributed in the membrane [30]. This implies that the labeled GM_1 molecules do not create clusters on their own but they do take part in interactions with the clusters once they are formed by the additional, unlabeled, GM_1. The same conclusion has been reached using the alternative FRET pair (Me)4bodipy-tail-labeled lipid (B7PC) as donor and r-GM_1 as acceptor [31].

The reported results were obtained with simulations where the domains in both bilayer leaflets are considered independent. Nonetheless, intra-leaflet contributions are usually less significant than the inter-leaflet ones and it was confirmed that domain coupling through the membrane provided similar results to non-coupled domains.

Parameters used for the Monte Carlo simulations regarding the g-/r-GM_1 FRET pair:
Förster radius: 5.9 nm
Donor mean lifetime in absence of acceptors: 5.5 ns
Distribution coefficients: Interestingly, the values of K_D and K_A did not influence the output parameters of the simulations in the entire investigated range (K = 1 - 10^6). Reduction of K gradually shallows the chi-squared minima, which for K < 10 totally disappears.

Supplementary Note 4
Lipid compositions

GUVs compositions in total mol% for samples containing GM_1.

Supplementary Table S24: FCS samples. Lipid dyes (DiD or g-GM_1) contribution is 0.0001% and therefore not included below for simplicity; all mentioned GM_1 is unlabeled.

Designation	Molar ratio
DOPC+2%GM_1 (100 +2%GM_1)	DOPC/GM_1: 98/2
DOPC+4%GM_1 (100 +4%GM_1)	DOPC/GM_1: 96.2/3.8
DOPC/Chol+2%GM_1 (75/25 +2%GM_1)	DOPC/Chol/GM_1: 73.5/24.5/2
DOPC/Chol+4%GM_1 (75/25 +4%GM_1)	DOPC/Chol/GM_1: 72.2/24/3.8
DOPC/Chol+2%GM_1 (65/35 +2%GM_1)	DOPC/Chol/GM_1: 63.7/34.3/2
DOPC/Chol+4%GM_1 (65/35 +4%GM_1)	DOPC/Chol/GM_1: 62.5/33.7/3.8
DOPC/Chol/Sph +4%GM_1 (70/25/5 +4%GM_1)	DOPC/Chol/Sph/GM_1: 67.3/24/4.8/3.8
DOPC/Chol/Sph +4%GM_1 (67/25/8 +4%GM_1)	DOPC/Chol/Sph/GM_1: 64.4/24/7.7/3.8
DOPC/Chol/Sph +4%GM_1 (65/25/10 +4%GM_1)	DOPC/Chol/Sph/GM_1: 62.5/24/9.6/3.8

Supplementary Table S25: FRET samples. Lipid dye pair g-GM_1/DiD.

Designation	Molar ratio
DOPC (100%DOPC)	DOPC/g-GM_1/DiD: 99.5/0.5/0.01
DOPC+1%$GM_{1\ unlabeled}$ (100+1%GM_1)	DOPC/GM_1/g-GM_1/DiD: 98.5/1/0.5/0.01
DOPC+2%$GM_{1\ unlabeled}$ (100+2%GM_1)	DOPC/GM_1/g-GM_1/DiD: 97.5/2/0.5/0.01
DOPC+4%$GM_{1\ unlabeled}$ (100+4%GM_1)	DOPC/GM_1/g-GM_1/DiD: 95.7/3.8/0.5/0.01
DOPC/Chol +1%$GM_{1\ unlabeled}$ (75/25 +1%GM_1)	DOPC/Chol/GM_1/g-GM_1/DiD: 73.9/24.6/1/0.5/0.01
DOPC/Chol +2%$GM_{1\ unlabeled}$ (75/25 +2%GM_1)	DOPC/Chol/GM_1/g-GM_1/DiD: 73.2/24.4/1.9/0.5/0.01
DOPC/Chol +4%$GM_{1\ unlabeled}$ (75/25 +4%GM_1)	DOPC/Chol/GM_1/g-GM_1/DiD: 71.8/23.9/3.8/0.5/0.01
DOPC/Chol/Sph +1%$GM_{1\ unlabeled}$ (70/25/5 +1%GM_1)	DOPC/Chol/GM_1/g-GM_1/DiD: 69/24.6/4.9/1/0.5/0.01
DOPC/Chol/Sph+2%$GM_{1\ unlabeled}$ (70/25/5+2%GM_1)	DOPC/Chol/GM_1/g-GM_1/DiD: 68.3/24.4/4.9/1.9/0.5/0.01
DOPC/Chol/Sph +4%$GM_{1\ unlabeled}$ (70/25/5 +4%GM_1)	DOPC/Chol/GM_1/g-GM_1/DiD: 67/23.9/4.8/3.8/0.5/0.01
DOPC/Chol/Sph +1%$GM_{1\ unlabeled}$ (67/25/8 +1%GM_1)	DOPC/Chol/GM_1/g-GM_1/DiD: 66/24.6/7.9/1/0.5/0.01
DOPC/Chol/Sph +2%$GM_{1\ unlabeled}$ (67/25/8 +2%GM_1)	DOPC/Chol/GM_1/g-GM_1/DiD: 65.4/24.4/7.8/1.9/0.5/0.01
DOPC/Chol/Sph +4%$GM_{1\ unlabeled}$ (67/25/8 +4%GM_1)	DOPC/Chol/GM_1/g-GM_1/DiD: 64.1/23.9/7.7/3.8/0.5/0.01
DOPC/Chol/Sph +1%$GM_{1\ unlabeled}$ (65/25/10 +1%GM_1)	DOPC/Chol/GM_1/g-GM_1/DiD: 64/24.6/9.8/1/0.5/0.01
DOPC/Chol/Sph +2%$GM_{1\ unlabeled}$ (65/25/10 +2%GM_1)	DOPC/Chol/GM_1/g-GM_1/DiD: 63.4/24.4/9.8/1.9/0.5/0.01
DOPC/Chol/Sph +4%$GM_{1\ unlabeled}$ (65/25/10 +4%GM_1)	DOPC/Chol/GM_1/g-GM_1/DiD: 62.2/23.9/9.6/3.8/0.5/0.01

Supplementary Table S26: FRET samples. Lipid dye pair g-GM_1/r-GM_1 (labels-GM_1).

Designation	Molar ratio
DOPC (100%DOPC)	DOPC/labels-GM_1: 99/1
DOPC+1%$GM_{1\ unlabeled}$ (100+1%GM_1)	DOPC/GM_1/labels-GM_1: 98/1/1
DOPC+2%$GM_{1\ unlabeled}$ (100+2%GM_1)	DOPC/GM_1/labels-GM_1: 97/2/1
DOPC+4%$GM_{1\ unlabeled}$ (100+4%GM_1)	DOPC/GM_1/labels-GM_1: 95.2/3.8/1
DOPC/Chol +1%$GM_{1\ unlabeled}$ (75/25 +1%GM_1)	DOPC/Chol/labels-GM_1: 73.5/24.5/1/1
DOPC/Chol +2%$GM_{1\ unlabeled}$ (75/25 +2%GM_1)	DOPC/Chol/labels-GM_1: 72.8/24.3/1.9/1
DOPC/Chol +4%$GM_{1\ unlabeled}$ (75/25 +4%GM_1)	DOPC/Chol/labels-GM_1: 71.4/23.8/3.8/1
DOPC/Chol/Sph +1%$GM_{1\ unlabeled}$ (70/25/5 +1%GM_1)	DOPC/Chol/GM_1/labels-GM_1: 68.6/24.5/4.9/1/1
DOPC/Chol/Sph +2%$GM_{1\ unlabeled}$ (70/25/5 +2%GM_1)	DOPC/Chol/GM_1/labels-GM_1: 68/24.3/4.8/1.9/1
DOPC/Chol/Sph +4%$GM_{1\ unlabeled}$ (70/25/5 +4%GM_1)	DOPC/Chol/GM_1/labels-GM_1: 66.7/23.8/4.8/3.8/1
DOPC/Chol/Sph +1%$GM_{1\ unlabeled}$ (67/25/8 +1%GM_1)	DOPC/Chol/GM_1/labels-GM_1: 65.7/24.5/7.8/1/1
DOPC/Chol/Sph +2%$GM_{1\ unlabeled}$ (67/25/8 +2%GM_1)	DOPC/Chol/GM_1/labels-GM_1: 65/24.3/7.8/1.9/1
DOPC/Chol/Sph +4%$GM_{1\ unlabeled}$ (67/25/8 +4%GM_1)	DOPC/Chol/GM_1/labels-GM_1: 63.8/23.8/7.6/3.8/1
DOPC/Chol/Sph +1%$GM_{1\ unlabeled}$ (65/25/10 +1%GM_1)	DOPC/Chol/GM_1/labels-GM_1: 63.7/24.5/9.8/1/1
DOPC/Chol/Sph +2%$GM_{1\ unlabeled}$ (65/25/10 +2%GM_1)	DOPC/Chol/GM_1/labels-GM_1: 63.1/24.3/9.7/1.9/1
DOPC/Chol/Sph +4%$GM_{1\ unlabeled}$ (65/25/10 +4%GM_1)	DOPC/Chol/GM_1/labels-GM_1: 61.9/23.8/9.5/3.8/1

References

[1] I. I. Mikhalyov, N. Gretskaya, L. B. Johansson, *Chem. Phys. Lipids* **2009**, *159*, 38–44.

[2] M. I. Angelova, S. Soléau, P. Méléard, F. Faucon, P. Bothorel, in *Trends Colloid Interface Sci. VI* (Eds.: C. Helm, M. Lösche, H. Möhwald), Steinkopff, Darmstadt, **1992**, pp. 127–131.

[3] P. Schuck, *Biophys. J.* **2000**, *78*, 1606–19.

[4] S. W. I. Siu, R. Vácha, P. Jungwirth, R. A. Böckmann, *J. Chem. Phys.* **2008**, *128*, DOI 10.1063/1.2897760.

[5] M. Manna, C. Mukhopadhyay, *PLoS One* **2013**, *8*, e71308.

[6] H. J. C. Berendsen, J. P. M. Postma, W. F. van Gunsteren, A. DiNola, J. R. Haak, *J. Chem. Phys.* **1984**, *81*, 3684.

[7] G. Bussi, D. Donadio, M. Parrinello, *J. Chem. Phys.* **2007**, *126*, 014101.

[8] T. Darden, D. York, L. Pedersen, *J. Chem. Phys.* **1993**, *98*, 10089.

[9] B. Hess, H. Bekker, H. J. C. Berendsen, J. G. E. M. Fraaije, *J. Comput. Chem.* **1997**, *18*, 1463–1472.

[10] S. Miyamoto, P. A. Kollman, *J. Comput. Chem.* **1992**, *13*, 952–962.

[11] S. Pronk, S. Pall, R. Schulz, P. Larsson, P. Bjelkmar, R. Apostolov, M. R. Shirts, J. C. Smith, P. M. Kasson, D. van der Spoel, et al., *Bioinformatics* **2013**, *29*, 845–854.

[12] S. Páll, M. J. Abraham, C. Kutzner, B. Hess, E. Lindahl, in *Solving Softw. Challenges Exascale*, **2015**, pp. 3–27.

[13] O. Berger, O. Edholm, F. Jähnig, *Biophys. J.* **1997**, *72*, 2002–2013.

[14] P. Niemelä, M. T. Hyvönen, I. Vattulainen, *Biophys. J.* **2004**, *87*, 2976–89.

[15] P. Jedlovszky, M. Sega, R. Vallauri, *J. Phys. Chem. B* **2009**, *113*, 4876–86.

[16] H. J. C. Berendsen, J. P. M. Postma, W. F. van Gunsteren, J. Hermans, in *Intermol. Forces* (Ed.: B. Pullman), **1981**, pp. 331–342.

[17] A. A. Polyansky, P. E. Volynsky, D. E. Nolde, A. S. Arseniev, R. G. Efremov, *J. Phys. Chem. B* **2005**, *109*, 15052–15059.

[18] M. Manna, C. Mukhopadhyay, *Phys. Chem. Chem. Phys.* **2011**, *13*, 20188.

[19] J. Danielsson, J. Jarvet, P. Damberg, A. Graslund, *Magn. Reson. Chem.* **2002**, *40*, S89–S97.

[20] E. Mombelli, R. Morris, W. Taylor, F. Fraternali, *Biophys. J.* **2003**, *84*, 1507–1517.

[21] R. M. Venable, A. J. Sodt, B. Rogaski, H. Rui, E. Hatcher, A. D. MacKerell, R. W. Pastor, J. B. Klauda, *Biophys. J.* **2014**, *107*, 134–145.

[22] A. Benda, M. Beneš, V. Mareček, A. Lhotský, W. T. Hermens, M. Hof, *Langmuir* **2003**, *19*, 4120–4126.

[23] F. Heinemann, V. Betaneli, F. A. Thomas, P. Schwille, *Langmuir* **2012**, *28*, 13395–13404.

[24] R. Macháň, M. Hof, *Biochim. Biophys. Acta* **2010**, *1798*, 1377–91.

[25] A. K. Smith, J. H. Freed, *J. Phys. Chem. B* **2009**, *113*, 3957–71.

[26] R. S. Petruzielo, F. a Heberle, P. Drazba, J. Katsaras, G. W. Feigenson, *Biochim. Biophys. Acta* **2013**, *1828*, 1302–13.

[27] F. A. Heberle, J. Wu, S. L. Goh, R. S. Petruzielo, G. W. Feigenson, *Biophys. J.* **2010**, *99*, 3309–18.

[28] J. Baumann, M. D. Fayer, *J. Chem. Phys.* **1986**, *85*, 4087.

[29] L. M. S. Loura, A. Fedorov, M. Prieto, *Biophys. J.* **2001**, *80*, 776–88.

[30] D. Marushchak, N. Gretskaya, I. I. Mikhalyov, L. B.-A. Johansson, *Mol. Membr. Biol.* **2007**, *24*, 102–12.

[31] R. Sachl, M. Amaro, G. Aydogan, A. Koukalová, I. I. Mikhalyov, I. A. Boldyrev, J. Humpolíčková, M. Hof, *Biochim. Biophys. Acta - Mol. Cell Res.* **2015**, *1853*, 850–857.